Correction to: Vacuum polarization and cyclotron resonance effects on radiative transfer and plasma deceleration in subcritical X-ray pulsars

by Ivan D. Markozov[1], Alexander Y. Potekhin[1], Alexander D. Kaminker[1] and Alexander A. Mushtukov[2,3]⋆
[1] *Ioffe Institute, Politekhnicheskaya 26, St Petersburg 194021, Russia*
[2] *Mullard Space Science Laboratory, University College London, Holmbury St. Mary, Surrey RH5 6NT, UK*
[3] *Astrophysics, Department of Physics, University of Oxford, Denys Wilkinson Building, Keble Road, Oxford OX1 3RH, UK*

4 November 2026

Key words: errata, addenda – accretion, accretion discs – radiative transfer – X-rays: binaries – stars: neutron

This is a correction to Markozov et al. (2026). In the originally published paper, optical depths were overestimated because of a technical error in the numerical code. Figure 1 shows an example of the correct effective optical depth $\tau_{\rm eff}$ as a function of photon energy E (the thick line) in comparison with the originally published one (the thin line, reproduced from Fig. 4 of the original paper). The correction weakens the plasma deceleration in the accretion channel near the neutron-star (NS) surface and consequently modifies the velocity profiles (Figs. 5–8 in the paper). These modifications are moderate, as we illustrate in Fig. 2. Here the thin lines reproduce the curves from original Fig. 6 for plasma velocity v in units of the speed of light c versus height above the NS surface at two accretion rates ($\dot{M} = 10^{15}$ g s^{-1} and 5×10^{15} g s^{-1}), and the thick lines show the corrected v/c profiles. Table 1 gives the corrected values of v/c at the NS surface for different model settings in comparison with the originally published ones.

In addition, curves in the original Figs. 9, 10, 13 (lower panel) and 14 (lower panel) were erroneously shifted along the vertical axes. All the corrections lead to modifications of Figs. 9–14. Here, Figs. 3–7 present the correct versions of Figs. 9, 10, 12, 13 and 14 (changes in Fig. 11 are insignificant, therefore we omit it). The values of the effective surface temperature in the captions have changed by ≈ 0.1–0.2 keV.

The reported corrections do not affect our qualitative results and conclusions. In particular, we confirm our original conclusions that the accretion flow braking is dominated by resonant Compton scattering and that the vacuum polarization is crucial for producing a strong cyclotron feature in the outgoing spectrum.

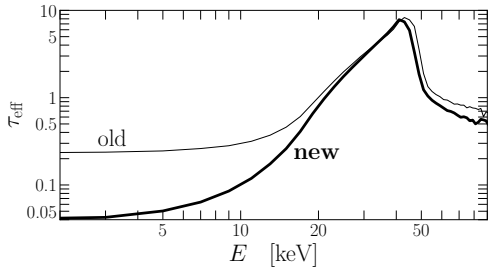

Figure 1: Uncorrected (thin curve) and corrected (thick curve) effective optical depth for all photons emitted in the upper hemisphere (angles to the channel axis $\vartheta \leq 90^\circ$) as a function of photon energy for the ring-shaped base of the accretion channel with radius $R_{\rm c} = 0.5$ km and thickness $d_{\rm w} = 15$ m at the mass accretion rate $\dot{M} = 2.5 \times 10^{15}$ g s^{-1} and cyclotron energy $E_B = 50$ keV. The scattering cross sections have been computed at mass density $\rho = 4 \times 10^{-4}$ g cm^{-3} and electron temperature $k_{\rm B}T = 5$ keV; the vacuum polarization has been taken into account.

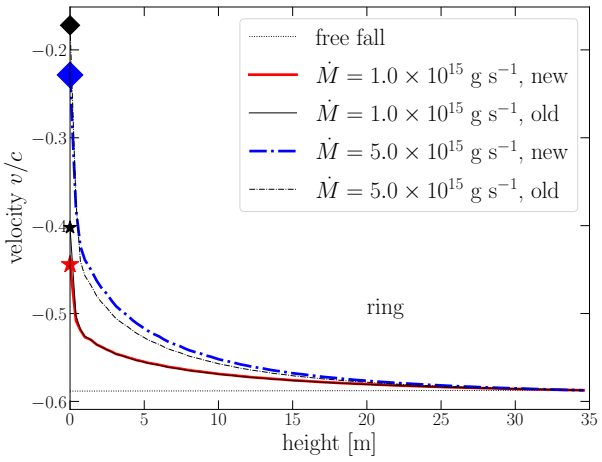

Figure 2: Illustration of corrections to the profiles of dimensionless plasma velocity v/c versus height above the hot polar cap of an NS emitting the blackbody radiation for the ring-shaped base of the accretion channel with radius $R_{\rm c} = 0.5$ km and thickness $d_{\rm w} = 15$ m at mass accretion rates $\dot{M} = 10^{15}$ g s^{-1} (two middle curves) and 5×10^{15} g s^{-1} (two upper curves). Vacuum polarization has been taken into account. The corrected profiles ('new', thick lines) are compared with the uncorrected ones that have been displayed in Fig. 6 of the original publication ('old', thin lines). The symbols at the left vertical axis visualize the v/c values attained at the NS surface according to Table 1. The dotted line shows the free-fall velocity.

⋆ E-mail: al.mushtukov@gmail.com

© 2026 The Authors

Table 1. *Corrected Table 1.* Dimensionless plasma velocity v/c at the NS surface for different accretion models: the circle or ring geometry of the accretion channel without (the 'plasma' model) or with (the 'vacuum' model) account of vacuum polarization effects, assuming either a complex model of the initial spectrum at the surface ('model boundary'; lines 9–11) or the blackbody initial spectrum (lines 2–8 and 12). The figure numbers in the first column refer to those in the original paper. The free-fall velocity is given in the first line. Corrected ('new') values of v/c are given along with the originally published ('old') ones.

line no.	Fig. no. (original)	model	$\dot{M}$ [10^{15} g s^{-1}]	$L_{\rm X}$ [10^{35} erg s^{-1}]	v/c new	v/c old
1	5–7	Free fall	Any	Any	−0.587	−0.587
2	5	Circle, plasma	1.0	1.55	−0.564	−0.520
3	5	Circle, vacuum	1.0	1.55	−0.561	−0.515
4	5	Circle, plasma	5.0	7.74	−0.463	−0.393
5	5	Circle, vacuum	5.0	7.74	−0.435	−0.366
6	6	Ring, vacuum	1.0	1.55	−0.444	−0.402
7	6	Ring, vacuum	2.5	3.87	−0.331	−0.282
8	6	Ring, vacuum	5.0	7.74	−0.229	−0.172
9	7	Model boundary	0.452	0.7	−0.491	−0.453
10	7	Model boundary	3.88	6.0	−0.387	−0.341
11	7	Model boundary	12.9	20	−0.326	−0.271
12	7	Blackbody	3.88	6.0	−0.244	−0.197

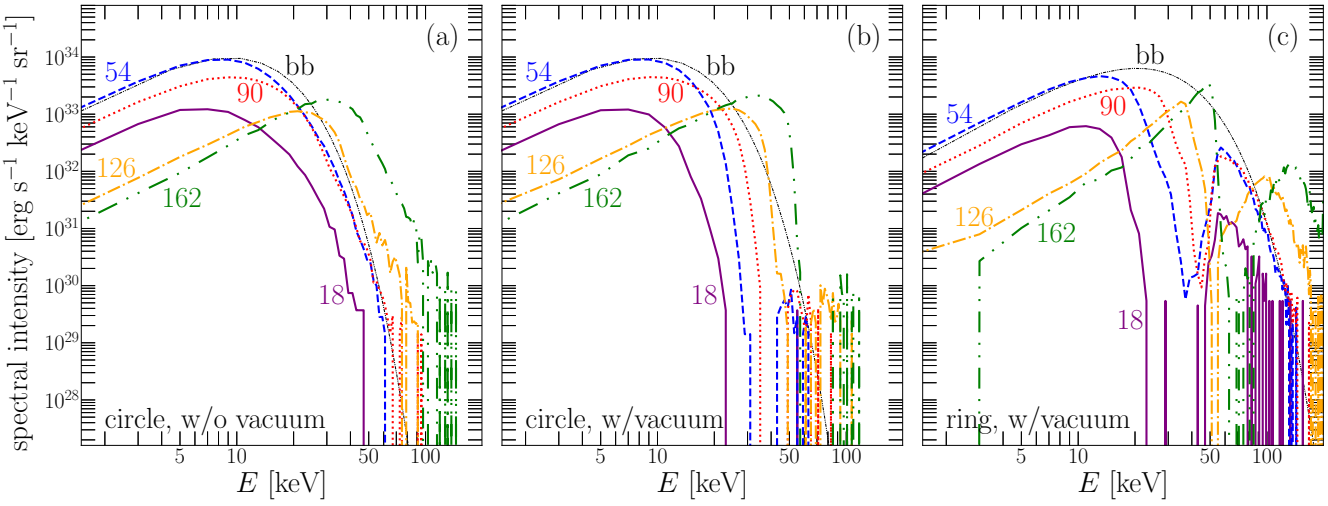

Figure 3. *Corrected Fig. 9.* Integrated intensity (i.e., spectral flux per unit solid angle) of radiation outgoing from an accretion channel at different angles ϑ to the channel axis as a function of photon energy E for the mass accretion rate $\dot{M} = 5 \times 10^{15}$ g s^{-1} and the electron cyclotron energy $E_B = 50$ keV, computed in three models: (a) the circle geometry and the collisionless plasma approximation neglecting vacuum polarization, (b) the circle geometry and the more accurate description of polarization according to equation (18), including the vacuum polarization effect and (c) the ring geometry with using the same description of the vacuum polarization effects, as in panel (b). The values of ϑ are marked near the curves: $\vartheta = 18°$ (solid line), 54° (dashed line), 90° (dotted line), 126° (dot-dashed line) and 162° (double-dot-dashed line). The thin double-dot-dashed curve marked 'bb' represents the blackbody integrated intensity emitted from the hot spot at the effective surface temperature $k_{\rm B}T_{\rm b} = 3.3$ keV and 7.3 keV in the cases of circle (panels a, b) and ring (panel c) geometries, without (panel a) and with (panels b, c) account of the vacuum polarization.

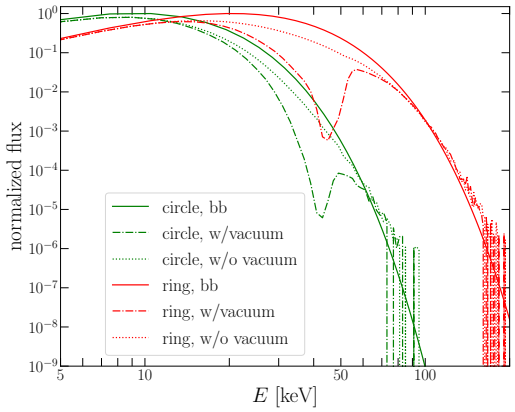

Figure 4. *Corrected Fig. 10.* Radiative spectral flux into the upper hemisphere as a function of photon energy for the circle (green curves with maxima at lower E) and ring (red curves with maxima at higher E) geometries of the accretion channel with the same parameters as in Fig. 3. The cases with (dot-dashed lines) and without (dotted lines) account of the vacuum polarization are shown. For each channel geometry, the curves are normalized to the maximum of the initial blackbody spectral flux from the surface, shown by the solid line, with effective temperatures $k_{\rm B}T_{\rm b} = 3.3$ keV in the case of circle geometry and 7.3 keV in the case of ring geometry.

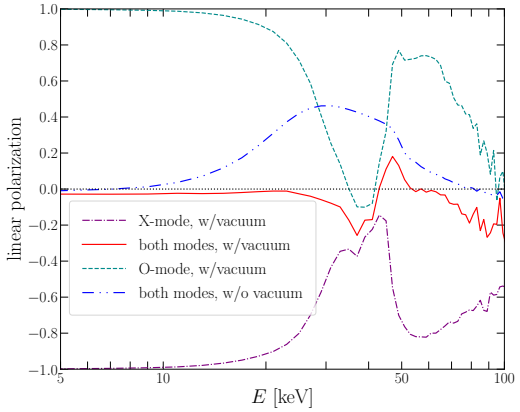

Figure 5. *Corrected Fig. 12.* Linear polarization degree P_L as a function of photon energy, averaged for radiation emitted into the upper hemisphere (with weights proportional to the total flux in each direction ϑ) for the ring geometry with $R_{\rm c} = 500$ m, $d_{\rm w} = 15$ m and accretion rate $\dot{M} = 2.5 \times 10^{15}$ g s^{-1}. The calculation of P_L including vacuum polarization effects (solid line) is compared with the cold collisionless plasma approximation neglecting the vacuum polarization (double-dot-dashed line), assuming unpolarized radiation from the NS surface. The dot-dashed (X-mode) and dashed (O-mode) curves show the results in the cases where the seed photons are injected in the channel in only one of the NMs, with the vacuum polarization effects taken into account.

REFERENCES

Markozov I. D., Potekhin A. Y., Kaminker A. D., Mushtukov A. A., 2026, MNRAS, 551, stag1517

This paper has been typeset from a TEX/LATEX file prepared by the author.

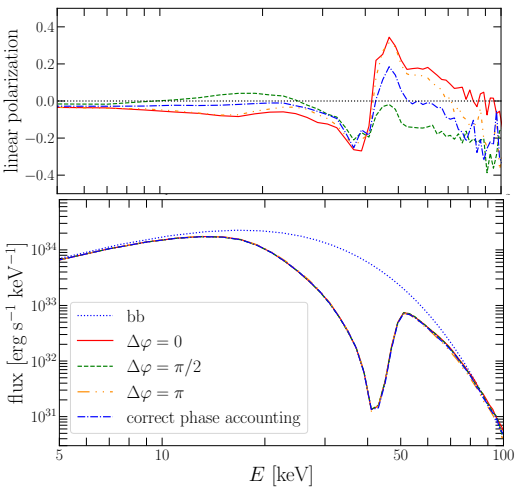

Figure 6. *Corrected Fig. 13.* Average linear polarization degree (*upper panel*) and flux (*lower panel*) of radiation emitted into the upper hemisphere in the ring geometry of the accretion channel with $R_{\rm c} = 500$ m and $d_{\rm w} = 15$ m as a function of photon energy for mass accretion rate $\dot{M} = 2.5 \times 10^{15}$ g s^{-1}, calculated using the cross sections with fixed azimuthal scattering angle $\Delta\varphi = 0$ (solid line), $\Delta\varphi = \pi/2$ (dashed line), $\Delta\varphi = \pi$ (double-dot–dashed line) and with the accurate $\Delta\varphi$ dependence (dot-dashed line). The vacuum polarization effects are included. The dotted line in the upper panel corresponds to zero polarization and the dotted line in the lower panel represents the spectrum of the blackbody radiation with $k_{\rm B}T = 5.9$ keV, which was used as the hot-spot boundary condition.

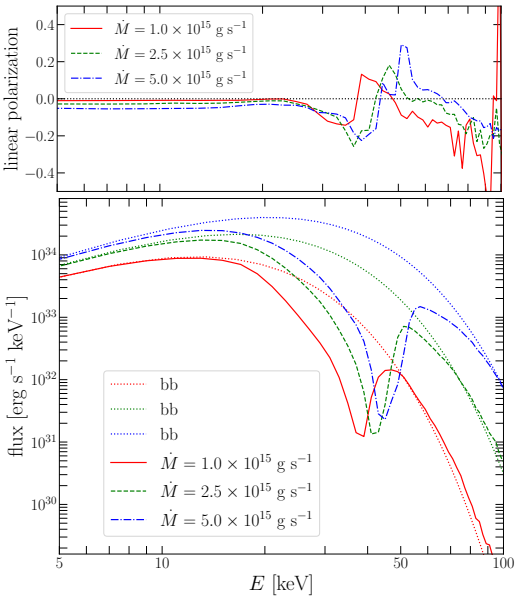

Figure 7. *Corrected Fig. 14.* Same as in the previous figure for mass accretion rates $\dot{M} = 10^{15}$ g s^{-1} (thick solid line), $\dot{M} = 2.5 \times 10^{15}$ g s^{-1} (dashed line) and $\dot{M} = 5.0 \times 10^{15}$ g s^{-1} (dashed-dotted line). The dotted lines in the lower panel represent the spectra of the blackbody radiation with (from bottom to top) $k_{\rm B}T = 4.5$ keV, 5.9 keV and 7.3 keV, which were used as the hot-spot boundary conditions.